Journal of Power Sources 221 (2013) 455–461

Contents lists available at SciVerse ScienceDirect

Journal of Power Sources

journal homepage: www.elsevier.com/locate/jpowsour

Improving microstructure of silicon/carbon nanofiber composites as a Li battery anode

Jane Y. Howe [a,*], David J. Burton [b], Yue Qi [c,**], Harry M. Meyer III [a], Maryam Nazri [b], G. Abbas Nazri [d], Andrew C. Palmer [b], Patrick D. Lake [b]

[a] Materials Sciences and Technology Division, Oak Ridge National Laboratory, Oak Ridge, TN 37831, USA
[b] Applied Sciences Inc., Cedarville, OH 45068, USA
[c] General Motors R&D, Warren, MI 48092, USA
[d] Physics Department, Wayne State University, Detroit 48202, USA

HIGHLIGHTS

- We report an interfacial study of a silicon/carbon nanofiber (Si/CNF) anode for Li-ion batteries.
- Amorphous Si layers were uniformly coated on both the exterior and interior walls of the hollow CNF.
- After cycling, more Si had fallen off from the outer wall than from the inner wall of CNF.
- Computer modeling suggests a higher interfacial strength at the Si/C interface at the inner wall.
- We proposed several interfacial engineering approaches to optimize the microstructure.

ARTICLE INFO

Article history:
Received 6 March 2012
Received in revised form
12 July 2012
Accepted 10 August 2012
Available online 21 August 2012

Keywords:
Silicon–carbon composite
Nanomaterial
Anode
Lithium-ion batteries

ABSTRACT

We report the interfacial study of a silicon/carbon nanofiber (Si/CNF) nanocomposite material as a potentially high performance anode for rechargeable lithium ion batteries. The carbon nanofiber is hollow, with a graphitic interior and turbostratic exterior. Amorphous silicon layers were uniformly coated via chemical vapor deposition on both the exterior and interior surfaces of the CNF. The resulting Si/CNF composites were tested as anodes for Li ion batteries and exhibited capacities near 800 mAh g^{-1} for 100 cycles. After cycling, we found that more Si had fallen off from the outer wall than from the inner wall of CNF. Theoretical calculations confirmed that this is due to a higher interfacial strength at the Si/C-edge interface at the inner wall than that of the Si/C-basal interface at the outer wall. Based upon the experimental analysis and theoretical calculation, we have proposed several interfacial engineering approaches to improve the performance of the electrodes by optimizing the microstructure of this nanocomposite.

1. Introduction

Carbon materials, usually in the form of graphite, are commonly used as the negative electrodes in secondary lithium ion batteries owing to their high cycle life and low cost. However, carbon negative electrodes have a theoretical capacity of 372 mAh g^{-1}, a typical practical energy capacity of ~300 mAh g^{-1} [1]. To boost the capacity of negative electrodes to meet the goals of the automotive industry for lithium ion batteries, researchers are investigating materials, which form alloys with lithium to generate negative electrodes that have specific capacities an order of magnitude higher than graphite. Silicon is an attractive negative electrode material for Li-ion batteries mainly because it has a very high theoretical charge capacity exceeding 3500 mAh g^{-1} [1]. However, the use of crystalline silicon as negative electrodes has been limited because silicon goes through large volume change and becomes amorphous after the first charge/discharge cycles. Recent work by Liu et al. [1] shows that pure silicon does collapse upon de-intercalation of lithium ions; this rapid volume change induces mechanical stress and fracturing (pulverization) of the Si particles, resulting in loss of electrical connection to the negative electrode structure and capacity fade.

In order to overcome these technical barriers, researchers have tried several approaches to combine the advantage of silicon's high capacity with carbon's high electrical conductivity and mechanical

* Corresponding author. Tel.: +1 865 386 9639; fax: +1 865 576 5413.
** Corresponding author.
E-mail addresses: jane.howe@gmail.com (J.Y. Howe), que.qi@gm.com (Y. Qi).

0378-7753/$ – see front matter © 2012 Elsevier B.V. All rights reserved.
http://dx.doi.org/10.1016/j.jpowsour.2012.08.026

strength. These approaches include: (1) producing nano-sized Si negative electrodes, either in particulate [2,3] or aligned nanowire form [5,6]; (2) making silicon/carbon composites in particulate form [3–7]; (3) coating tubular-forms of carbon with silicon [8–10,12]; and (4) putting a carbon coating on silicon nanowires [11]. These research efforts demonstrated that nanoscale silicon/carbon composites are able to accommodate larger strains than the bulk silicon and thus reduce the extent of pulverization, provide good electronic contact and conduction, and display short lithium insertion distances.

A structurally superior design would be to develop silicon-coated hollow carbon nanofibers as the negative electrode material for Li-ion batteries. The attractive properties of catalytically grown carbon nanofibers (CNF) have been known for decades [13,14]. They can be mass-produced inexpensively, have excellent mechanical strength, and high thermal and electrical conductivity [15]. The CNF produced by Applied Sciences Inc. (Cedarville, OH) has a water hose-like morphology. About 30–100 um in length, it has an outer diameter of 100–200 nm and a hollow core typically about 1/3–1/2 of the total fiber diameter. To make a Si/CNF composite, Applied Sciences Inc. uses chemical vapor deposition of nano-scale coatings of amorphous silicon on both the interior and exterior surfaces of the hollow CNF. Battery tests have shown that capacities about 800 mAh g^{-1} for 100 cycles in half-cell and full cell configuration have been achieved. The Coulombic efficiency of these negative electrodes has been measured to be 99% after SEI formation being stabilized in several cycles. In this paper, we report the failure analysis of the Si/Carbon nanofiber nanocomposite as a negative electrode material after cycling; and further provide pathways for improving the cycling performance based upon the unique microstructures of these Si/CNF composites.

2. Materials and experimental procedures

2.1. Fabrication of Si/CNF nanocomposites

A nanoscale layer of silicon was deposited onto a highly graphitic carbon nanofiber (Pyrograf®-III, PR-25-XT-PS and HHT, Pyrograf Products, Inc., Cedarville, OH) through a chemical vapor deposition process. The source of silicon was a silane gas blended in a non-reactive carrier gas. The silicon was deposited onto a powdered form of carbon nanofiber at elevated temperatures (400–700 °C) using either a horizontal bed reactor with a static target or in a fluidized bed reactor. The thickness, crystallinity, and morphology of the silicon are adjustable through alterations in the coating parameters. For this research, the silicon to carbon ratio (by weight) of 1:3 was targeted to provide a specific negative electrode capacity of about 900 mAh g^{-1}.

2.2. Half-cell and full-cell battery tests

Electrodes were produced from a thick slurry paste that contained 80 wt% silicon coated CNF powder as the active material, with 15 wt% PVDF (polyvinylidene fluoride) binder dissolved in NMP (N-Methyl Pyrrolidone) and 5 wt% conductive carbon black. The mass of conductive carbon black was excluded while calculating the capacity. A 20-micron thick coating of the paste was applied to a 10-micron thick copper foil using a doctor blade drawdown technique. The electrodes were pre-dried inside a well-ventilated hood and then transferred to a hot antechamber (110 °C) of a dry box and evacuated for at least 4 h. The dry sample was transferred to the inside of the dry box that was filled with argon, with less than 1 ppm of oxygen and moisture. Disks were cut from the coated copper foil and inserted into the coin cells.

Half and full cells were manufactured with the silicon coated carbon nanofibers. The half cells were constructed with the Si–CNF powder as the cathode and lithium metal as the negative electrode. The half cells were cycled from 2.5 V to 0.010 V. Full cells were constructed with the Si–CNF product as the negative electrode and $LiCoO_2$ as the cathode. Full cells were cycled from 4.3 V to 2.7 V. The performance of the carbon–silicon negative electrode was measured at different C rates ranging from C/15 to 1C. All cells used an electrolyte consisting of a multi-blend solvent (a combination of dimethyl carbonate and ethylene carbonate with a vinylene carbonate additive) containing 1 M $LiPF_6$.

2.3. Materials characterization of the Si/CNF composites

The Si/CNF composites were analyzed before and after the coin cell tests using electron microscopy, energy-dispersive X-ray spectroscopy (EDS), and X-ray photoelectron spectroscopy (XPS). For the microscopy study, the Si/CNF composite specimens were dispersed onto a lacey carbon film supported on a 200-mesh Cu grid without using any dispersing agent, then analyzed using a Hitachi HF-3300 TEM/STEM equipped with a Thermo Noran Si(Li) EDS detector at 300 kV. The XPS study, with samples mounted on the stainless steel sample carrier using double-sided tape, was carried out by a Thermo Fisher Scientific K-Alpha XPS using monochromatic Al K-alfa x-rays. Ar-ion sputter profiling was attempted as a way of showing changes in surface chemistry as a function of depth. Profiles were generated by intermittently sputtering the sample surface with 3 kV Ar-ions and then collecting a set of core level data. The Avantage Software package (v. 4.44) was used for all XPS data acquisition and analysis.

3. Results and discussions

3.1. Electrochemical evaluations

Half-cell performance data – Samples of the silicon coated carbon nanofiber were converted into an electrode and countered with lithium metal in a coin cell. The cell was cycled from 2.5 V to 0.010 V at rate of C/2 with no formation cycle performed to intentionally create an SEI layer. Fig. 1 contains the delithiation-capacity, showing that the initial specific capacity of the composite material was 1100 mAh g^{-1} and decayed to 750 mAh g^{-1} after 100 charge/discharge cycles. We attribute the irreversible capacity to the initial breakdown of the Si/CNF composite and the formation of the SEI layer. The Coulombic efficiency was measured to be 99% after SEI formation being stabilized in several cycles. Post cycling analysis of the composite material was performed to

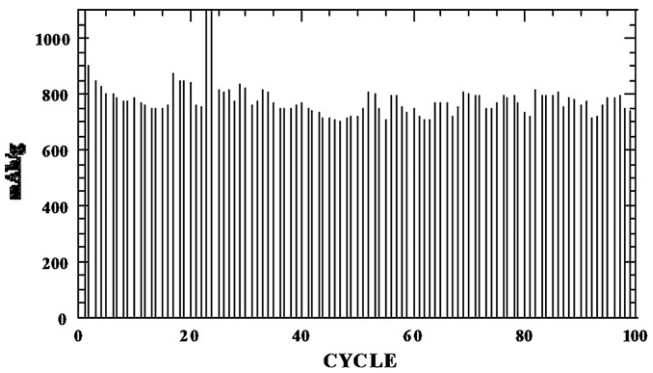

Fig. 1. Specific capacity of silicon coated carbon nanofiber against Li metal in coin cell (Delithiation of the Si/CNF in half-cell configuration).

evaluate the condition of the Si/CNF nanocomposites (Section 3.3). These structural characterization indicate that the capacity decay is a result of material degradation at the Si/CNF electrodes, specifically at the interface of the Si/CNF composites.

Full-cell performance data – Silicon coated nanofiber powder was also tested in a full cell configuration to characterize the performance of the high capacity negative electrode against conventional cathode materials. Coin cells were fabricated using the composite material as the negative electrode and $LiCoO_2$ as the cathode. Capacity was calculated based upon the total mass of the Si/CNF composites but excluding the carbon black additive. The initial specific capacity of the negative electrode was near 1000 mAh g^{-1} for charging and ~800 mAh g^{-1} for discharging, providing a charging and discharging profile similar to those used in typical graphite electrode across a voltage range of 4.2–2.8 V as shown in Fig. 2.

We compare the electrochemical performance data with that from other forms of silicon/carbon nanocomposites. Cui reported the initial capacity of their Si-coated carbon nanowire to be 2200 mAh g^{-1} but with a Coulombic retention efficiency at 96% [10]. Kim et al. reported that carbon-coated silicon particles with an average size of 10 nm had a capacity over 3000 mAh g^{-1} with an efficiency at 98% [3]. The Si/CNF in this study has a lower initial capacity due to the low fraction of silicon in the composite. However, it has a higher retention efficiency than carbon-coated silicon particle and Si-coated carbon nanowire, likely due the unique microstructure of this silicon-coated, hollow carbon nanofiber (more discussions in Section 3.3).

3.2. Understanding the microstructure through electron microscopy and XPS analysis

Electron microscopy was used in conjunction with energy dispersion spectroscopy (EDS) to characterize the microstructure and crystallinity of the composites, and the interface between the carbon nanofibers and the deposited silicon. Surface information of the composites was analyzed using XPS. The TEM bright field (BF) signals contain information of crystallinity (phase) and mass-thickness contrast. The Z-contrast (ZC) image, collected using a high-angle annular dark field detector, has a contrast proportional to Z^2 (Z is the atomic number). Using a TEM/STEM equipped with a scanning system for the detection of secondary electrons, it enables high-resolution micrographs to be recorded in BF, ZC, and SE modes from the *same* region of interest. The combination of the three electron signals allows a more comprehensive understanding of the microstructures of the composites.

Before discussing the Si/carbon nanofiber composites, it is necessary to give a detailed description of the unique microstructures of the carbon nanofiber used in this study. The Pyograf®-III carbon nanofibers were produced through a two-stage vapor growth processes [14,16]. First, the "catalytic phase" is formed, in which layers of graphitic carbon grow at the interface of the catalytic iron particle. Then the fiber is thickened by pyrolytic deposition of carbon. The resulting CNF is 30–100 um long, with an outer diameter of 100–200 nm and a hollow core typically about 1/3–1/2 of the total fiber diameter. As shown in Fig. 3, the interior of the carbon fiber is more graphitic, with the nesting planes canted at about 15°–25° angle from the longitudinal fiber axis [16]. The pyrolytically deposited outer layer is less ordered; and the turbostratic carbon planes are, on average, parallel to the fiber axis. It is obvious that this kind of CNF is very different from multi-walled carbon nanotubes (MWNTs) in two aspects: (1) the CNFs have much larger diameter than that of MWNTs, which are normally less than 20 nm OD; and (2) a MWNT does not have a hollow core of tens of nm in diameter.

The Si/CNF composites were then fabricated by thermally decomposing silane and depositing silicon onto the surfaces of the CNFs. Illustrated in Fig. 4, silicon layers formed on both interior and exterior surfaces of the CNFs. By adjusting the deposition parameters, silicon may form a discontinuous coating or full coverage on both internal and external surfaces of the CNFs. In Fig. 5, the SEM reveals a uniform, partial coverage as sub-20 nm silicon nodules decorated both the interior and exterior surfaces. Fig. 6 shows that silicon formed continuous and complete layers on the external and internal surfaces. The presence of silicon on the inner surface of hollow CNF was clearly revealed in the Z-contrast image of Fig. 6b, as the high-Z silicon was bright. Chemical composition of the Si/CNF was obtained from the EDS line scan across the fiber. The profile in Fig. 6d showed a Si-rich outer surface, which does not contain carbon, suggesting the presence of a continuous *pure* silicon outer layer. The regions corresponding to the inner surface also have a high concentration of Si. In order to positively identify the presence of a pure inner Si layer, we compared the structural features of the outer and inner layers in the high-resolution BF image (Fig. 4): both are amorphous and bear similar features. The EDS line scan shows oxygen to be near or below the detection limit. From both EDS line scan profiles and ZC or BF images, we can measure the thickness of the silicon layers. In Fig. 4, the inner layer is about 15 nm and an outer layer about 10 nm. The SEM image revealed the granular nature of the silicon coating.

The chemical analysis was further conducted using X-ray photoelectron spectroscopy (XPS). Fig. 7 presents XPS spectra of the

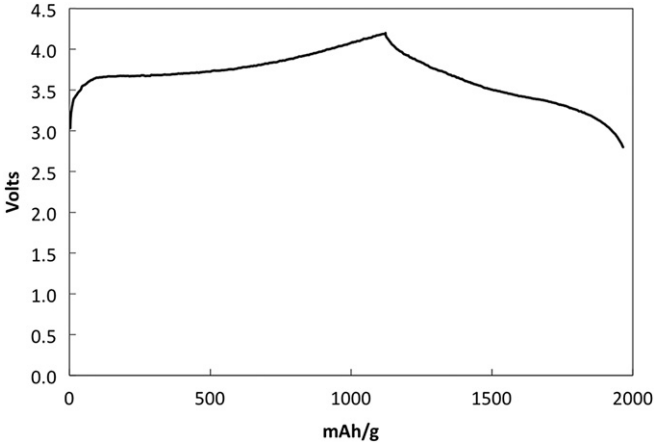

Fig. 2. Initial cycle of full cell with silicon coated nanofiber as the negative electrode and $LiCoO_2$ as the cathode.

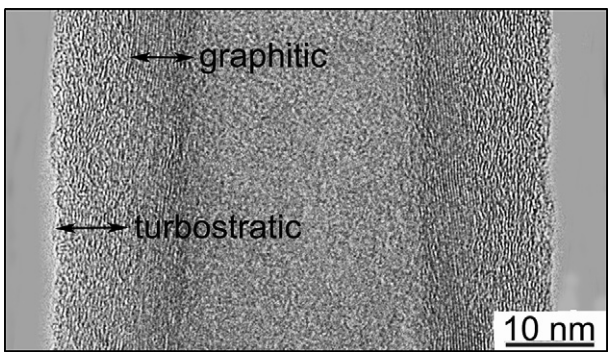

Fig. 3. Microstructure of the hollow-cored carbon nanofiber. The interior is more graphitic and the outer layer is turbostratic.

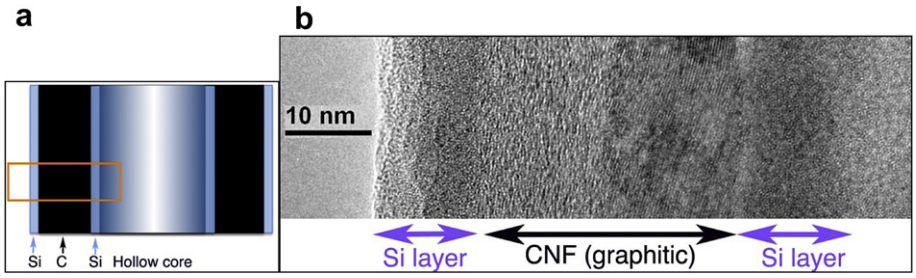

Fig. 4. (a) The schematic illustrates the layered structure of Si/CNF; and (b) Bright-field TEM reveals the amorphous Si on both inner and outer surfaces of CNF of an outlined area as in (a).

Si/CNF before and after the cycling tests. On the left hand side in Fig. 7a, three wide energy survey scans are shown for the material before cycling. Each spectrum represents a different area and shows there is a small spot-to-spot variation. The core level spectra (narrow energy range scans) for C, Si, and O were also obtained, but are not presented. These spectra showed: (1) a primary C peak at ~285 eV binding energy, which is the binding energy (BE) related to the C-fiber; (2) a primary peak at ~99 eV BE for Si plus a smaller peak at ~103 eV BE from oxidized Si; and (3) an O peak centered at ~532 eV BE consistent with Si–O bonding. The survey spectra on the right hand side of Fig. 7b were taken on material after cycling. In addition to C, Si, and O, Li, F, and P were also detected. It is clear, even in the survey spectra, that the C now shows two prominent features. Core level spectra for C, Si, Li, F, O, and P were obtained for the cycled material, but are not presented. Indeed, the C 1s spectrum showed that in addition to the C-fiber feature at ~285 eV, a second peak was observed at ~290 eV BE that is related to lithium carbonate. The Si 2p core level spectrum was a much weaker signal for the cycled material due to the lithium carbonate overlayer and showed that the detected Si was mainly present as oxidized silicon. Significantly, no features were found in the C 1s core level spectra for either material related to SiC formation, i.e. no peak at ~282–283 eV was observed. Absence of silicon–carbide type of binding energies in these profile is consistent with the TEM analysis that there is no silicon carbide at the interface of amorphous silicon and carbon nanofibers.

3.3. Microstructural analysis of the Si/CNF negative electrode material after battery tests

Negative electrode materials removed from the coin cell after cycling tests were analyzed using XPS and STEM. The XPS spectra in Fig. 7b revealed lithiated surfaces. Fluorine and phosphorous peaks were from the residuals of electrolyte. Microstructures of electrodes ended with low capacity were presented in Fig. 8. In Fig. 8a, the SEM micrograph of a Si/CNF reveals very little Si coating on the exterior. Before the cycling test, these fibers had a continuous layer of silicon as shown in Fig. 6a. After the cycling test, the ZC micrograph in Fig. 8b revealed that much more Si had fallen off from the outer wall than the inner wall of CNF. Recalling that the capacity curve (Fig. 1) stayed related flat throughout the 10–100 cycles at ~750 mAh g^{-1}. Our calculation suggested that if the Si has completely delaminated from the outer surface of CNF, the cell capacity would be much less 750 mAh g^{-1}. This concurs that the severe morphological change shown in Fig. 8 which correlates to the failure stage of the electrodes. An *in situ* study is on-going to better understand the relationship of morphological evolution during cycling.

For the postmortem analysis, it is of great interest to understand whether the preferential removal of Si on the outer surface of CNF is related to the intrinsic Si/C interfacial strength due to different orientations of graphite planes in CNF. Because the CNF has graphitic inner core and turbostratic exterior, it renders slight different Si/CNF interfaces at interior and exterior. To further illustrate this point, we constructed two atomic Si/C interfaces structure to mimic different interface formed between Si and the outer wall and inner of the CNF, and computed their interface strength from density functional theory (DFT) calculations.

Although the outer layer is less ordered; it is considered to be comprised of turbostratic carbon planes, on average, parallel to the fiber axis. Since turbostratic carbon is mainly sp^2 bonded carbon atoms, which can be considered as graphite planes stacked in a disordered manner, it is reasonable to represent this surface with graphite basal planes for the current quantum calculations. Fig. 9a shows the relaxed Si/C-basal interface, consisting of a 10 Å thick amorphous Si slab and a 4-layer graphite (001) slab with 10 Å vacuum layer. The 2D periodic boundary condition used in the slab interface model assumes the basal planes to be flat, which underestimates the slight curvature (1/100–200 nm) of a graphite plane on the outer wall of a real CNF. To mimic the interface between the inner wall of CNF and Si, the Si/C-edge interface was constructed by rotating the graphite (001) planes 38.6° to expose the edge sites on graphite (012) planes to amorphous Si (The canting angle of 38.6° is larger than that found in the actual CNF of 25° or less; it is

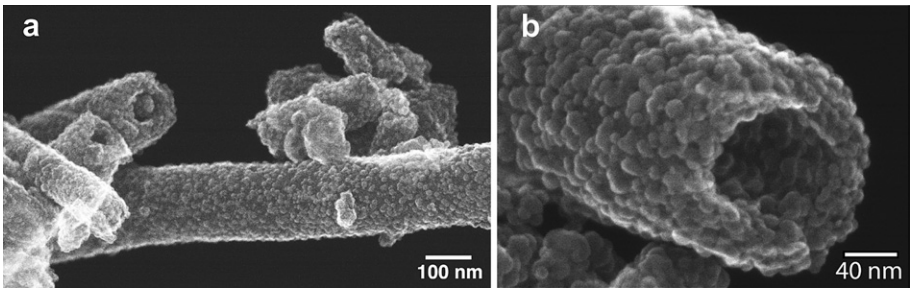

Fig. 5. SEM images of the silicon/CNF composite: uniformly distributed nanosized Si nodules on the exterior and interior surface of CNFs.

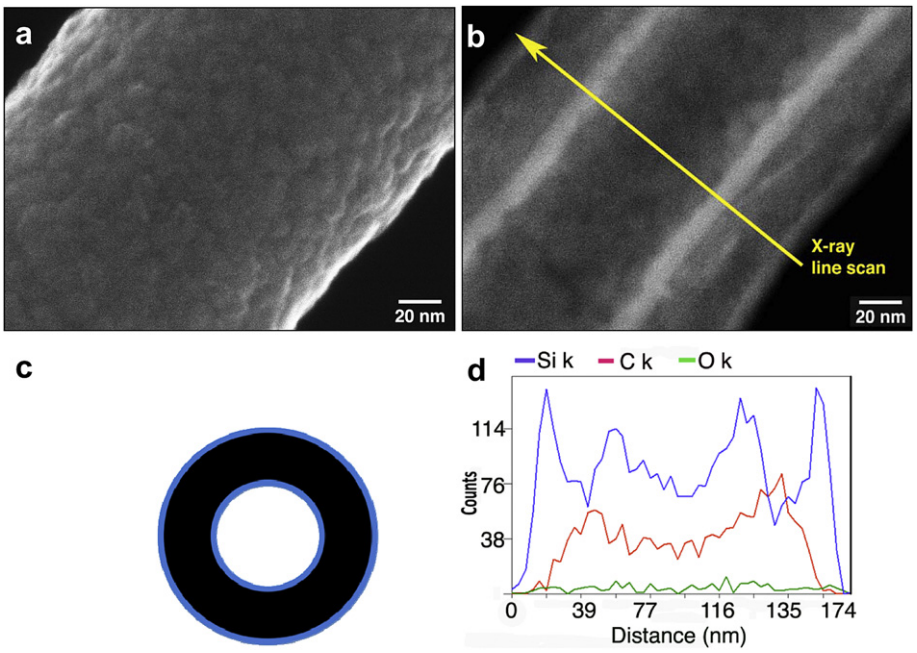

Fig. 6. Continuous silicon layer over the internal and external surfaces of a CNT: (a) an SEM image; (b) a Z-contrast image of the same area where the silicon coatings are bright; (c) a schematic of the cross-sectional view of a Si/CNF, showing Si layers on both interior and exterior; and (d) the EDS line-scan across the fiber revealing the concentration and distribution of Si, C, and O.

a compromise for constructing a sizable supercell that requires reasonable computation time.). For this slab model, the carbon atoms on the free surface were saturated with hydrogen atoms. In both interface structures, the amorphous Si (64 atoms) was pre-formed by melting and quenching crystalline Si structures using *ab initio* molecular dynamics [17].

All DFT calculations were performed using the Vienna Ab Initio Simulation (VASP) Package [18,19] with the Projector Augmented Wave (PAW) method and the Perdew–Burke–Ernzerhof (PBE) form of the local gradient approximation (LDA) for exchange and correlation. From convergence studies, we determined the kinetic energy cutoff in the plane wave expansion to be 400 eV and a gamma-centered $3 \times 3 \times 1$ k-mesh for the slab modeled. The relaxed interface structure in Fig. 9 clearly shows that Si forms more bond with graphite edge sites (at the inner wall of CNF) than with carbon basal planes (at the outer wall of CNF). We also computed the equilibrium work of separation (W_{sep}) by comparing the energy difference between the interface and the separated Si and carbon slabs. Due to the lack of atomic bonding at the Si/C-basal interface, its W_{sep} is only 0.11 J m^{-2}, much smaller than $W_{sep} = 3.05$ J m^{-2} at Si/C-edge interface. At the Si/C-basal interface, the nearest distance between Si and C is 2.8–2.9 Å. In comparison, at the Si/C-edge interface, there are much more Si–C bond with a distance around 1.8 ~ 1.9 Å, similar to the Si–C bond distance in crystalline SiC. Although the Si/C-basal interface is weak, it's actually still stronger than the cohesion energy between graphite basal planes, as the basal plane distance is 3.3 Å and its W_{sep} is around 0.074 J m^{-2} [20]. In an *ab-inito* molecular dynamics simulation of the Si/C-basal interface at 1000 K, we noticed that one layer of graphite peeled off with the Si slab during film delamination, consistent with the fact that the W_{sep} at the Si/C-basal interface is stronger than the cohesion energy of graphite basal planes. However, this may not

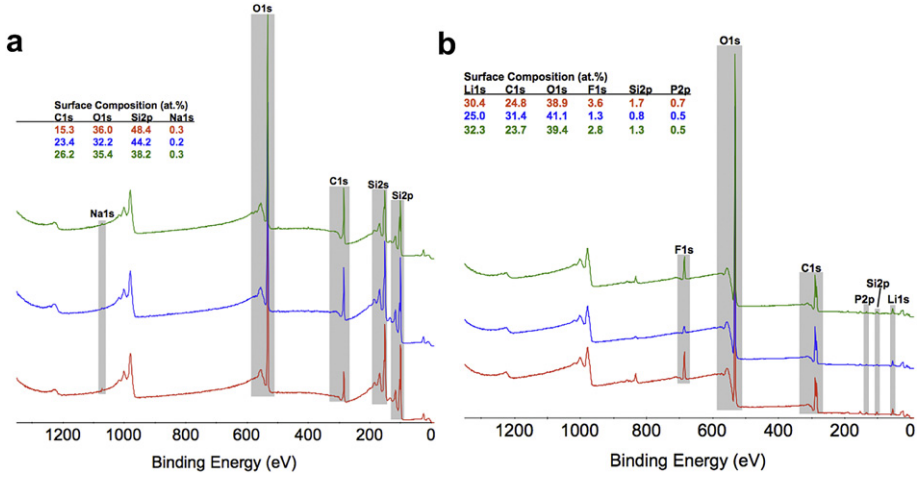

Fig. 7. XPS analysis of the Si/CNF before (a) and after the cycling tests (b).

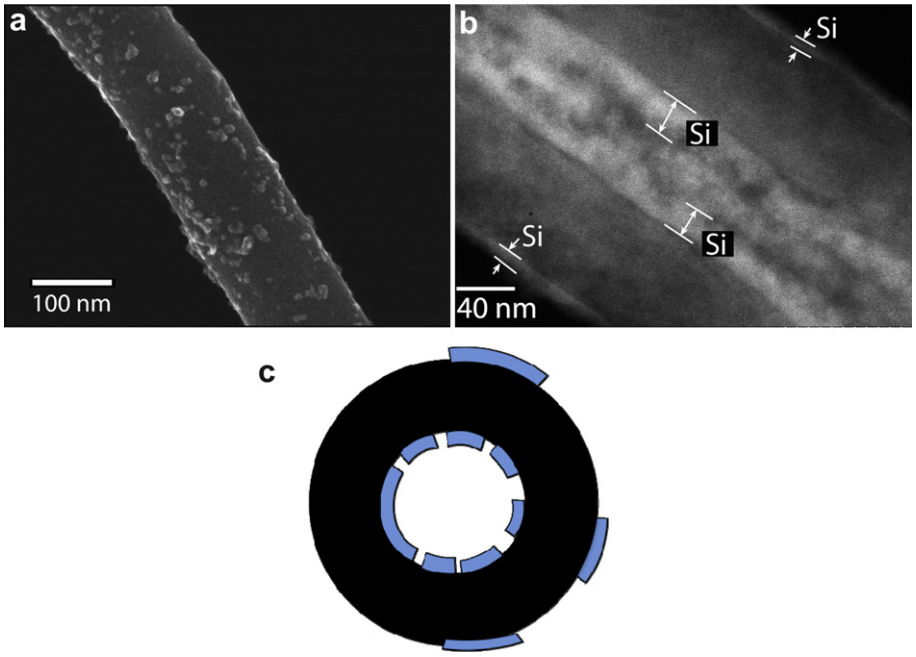

Fig. 8. Microstructure of Si/CNF after cycling tests: (a) an SEM image reveals the uneven distribution of Si nodules on the outer surface; (b) a Z-contrast micrograph shows the hollow core is filled with pulverized silicon nanoparticles; and (c) a schematic illustrates that the cross-sectional view of a hollow core contains the silicon pieces.

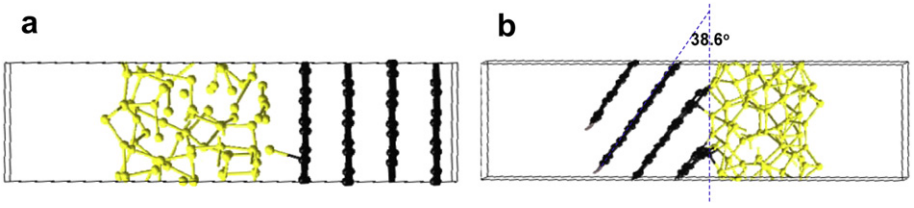

Fig. 9. Supercell constructed for the DFT simulation: relaxed interface structure of amorphous Si on (a) graphite basal planes and (b) graphite tilted edges 38.6°, where black atoms are carbon and yellow atoms are Si. (For interpretation of the references to color in this figure legend, the reader is referred to the web version of this article.)

happen in CNF, if the outer most graphite plane is a continuous cylinder. Thus, the simulation offered a convincing explanation that less Si fell off from the inner surface than the outer surface due to a higher interfacial energy of the Si/C-edge interface than that of the Si/C-basal interface.

Based upon the experimental analysis and theoretical calculation, we propose several pathways for improving the performance of the electrodes by optimizing the microstructures. One obvious improvement is to protect the outer Si coating by adding a protective overcoat. The interfacial strength of Si/CNF can also be improved by either exposing more sp^3 carbon on the surface or chemically modifying the surface of the CNF before depositing Si layers.

4. Conclusions

The novel Si/CNF composites have amorphous silicon coatings on both internal and external surfaces of the hollow CNFs. This Si/CNF composite has many unique features that, we believe, lead to a promising cycling performance. Having silicon coatings on both inner and outer surfaces of a hollow carbon nanofiber improves the capacity of the Si/CNF composite during cycling. The hollow core of the CNF effectively moderates the degradation of the Si negative electrode. We observed that more Si had fallen off from the outer wall than the inner wall of CNF after cycling, likely due to the stronger Si/C interfacial bonding at the inner wall, as suggested by the computational study. Learning this, we are working on several interfacial engineering approaches as proposed above to improve the structure of the Si/CNF for the optimal performance.

Acknowledgments

This research at the Oak Ridge National Laboratory's High Temperature Materials Laboratory User Program was sponsored by the U.S. Department of Energy, Office of Energy Efficiency and Renewable Energy, Vehicle Technologies Program. We thank Dr. Meng Jiang of GM for the insightful discussions.

References

[1] X.H. Liu, L.Q. Zhang, L. Zhong, Y. Liu, H. Zheng, J.W. Wang, et al., Nano Lett. 11 (6) (2011 Jun) 2251–2258.
[2] H. Li, X.J. Huang, L.Q. Chen, G.W. Zhou, Z. Zhang, D.P. Yu, et al., Solid State Ionics 135 (1–4) (2000 Nov) 181–191.
[3] H. Kim, M. Seo, M.H. Park, J. Cho, Angew. Chem., Int. Ed. 49 (12) (2010) 2146–2149.
[4] S.M. Jang, J. Miyawaki, M. Tsuji, I. Mochida, S.H. Yoon, Carbon 47 (15) (2009 Dec) 3383–3391.
[5] S.H. Ng, J. Wang, D. Wexler, S.Y. Chew, H.K. Liu, J. Phys. Chem. C 111 (29) (2007 Jul 26) 11131–11138.
[6] J.S. Xue, K. Myrtle, J.R. Dahn, J. Electrochem Soc. 142 (9) (1995 Sep) 2927–2935.
[7] J. Yang, B.F. Wang, K. Wang, Y. Liu, J.Y. Xie, Z.S. Wen, Electrochem Solid-State Lett. 6 (8) (2003 Aug) A154–A156.
[8] L.F. Cui, L.B. Hu, J.W. Choi, Y. Cui, ACS Nano 4 (7) (2010 Jul) 3671–3678.

[9] L.F. Cui, R. Ruffo, C.K. Chan, H.L. Peng, Y. Cui, Nano Lett. 9 (1) (2009 Jan) 491–495.
[10] L.F. Cui, Y. Yang, C.M. Hsu, Y. Cui, Nano Lett. 9 (9) (2009 Sep) 3370–3374.
[11] R. Huang, X. Fan, W. Shen, J. Zhu, Appl. Phys. Lett. 95 (13) (2009 Nov) 113119–113121.
[12] W. Wang, P.N. Kumta, ACS Nano 4 (4) (2010 Apr) 2233–2241.
[13] G.G. Tibbetts, J. Cryst. Growth 66 (3) (1984) 632–638.
[14] G.G. Tibbetts, G.L. Doll, D.W. Gorkiewicz, J.J. Moleski, T.A. Perry, C.J. Dasch, et al., Carbon 31 (7) (1993) 1039–1047.
[15] J.Y. Howe, G.G. Tibbetts, C. Kwag, M.L. Lake, J. Mater. Res. 21 (10) (2006 Oct) 2646–2652.
[16] G.G. Tibbetts, M.L. Lake, K.L. Strong, B.P. Rice, Compos. Sci. Technol. 67 (7–8) (2007) 10.
[17] V.B. Shenoy, P. Johari, Y. Qi, J. Power Sources 195 (19) (2010 Oct 1) 6825–6830.
[18] G. Kresse, J. Furthmüller, Comput. Mater. Sci. 6 (1) (1996) 15–50.
[19] G. Kresse, J. Furthmüller, Phys. Rev. B 54 (16) (1996) 11169–11186.
[20] Y. Qi, L.G. Hector, N. Ooi, J.B. Adams, Surf. Sci. 581 (2–3) (2005 May 1) 155–168.